Available online at www.sciencedirect.com
ScienceDirect
Ceramics International 37 (2011) 731–739
CERAMICS INTERNATIONAL
www.elsevier.com/locate/ceramint

Correlation of compaction pressure, green density, pore size distribution and sintering temperature of a nano-crystalline 2Y-TZP-Al_2O_3 composite

Soumyajit Koley, Abhijit Ghosh [1], Ashok Kumar Sahu *, Raghavendra Tewari, Ashok Kumar Suri

Materials Group, Bhabha Atomic Research Centre, Mumbai, India

Received 6 November 2009; received in revised form 3 September 2010; accepted 28 September 2010
Available online 1 December 2010

Abstract

Highly sinter-active nano crystalline composite powder of 2 mol% yttria doped tetragonal zirconia polycrystal (2Y-TZP) with 2 wt% alumina was synthesized by co-precipitation method. Crystallization temperature of the amorphous precursor powder, measured from simultaneous thermogravimetric (TG) and differential thermal analysis (DTA) techniques was found to be ~470 °C. The powder was calcined at different temperatures in the range of 700–1000 °C. XRD patterns of the calcined powders revealed the presence of a single tetragonal phase. Particle size of the calcined powder measured by different techniques (X-ray line broadening, BET surface area and laser scattering technique) indicated an increase in the average particle size with calcination temperature. The study of compaction behaviour revealed the presence of soft agglomerates in the calcined powder. Pore size distribution of the green compacts obtained from a mercury porosimeter was found to be monomodal above a critical pressure. The onset temperature of sintering was found to increase with calcination temperature. Powders calcined at 800 °C and 900 °C had shown better sinterability at 1200 °C owing to the presence of finer pores with a narrow size distribution in the green compacts. Sintering behaviour of the powder calcined at 700 °C was found to be marginally poorer in comparison to the other samples, whereas the powder calcined at 800 °C had demonstrated best densification behaviour, especially when compacted at 300 MPa.

Keywords: A. Sintering; B. Nanocomposite; Agglomeration/agglomerates; Zirconia:yttria-stabilized tetragonal polycrystal

1. Introduction

Yttria stabilized tetragonal zirconia polycrystal (Y-TZP) has been proved to be an important structural ceramic owing to its excellent mechanical properties viz. high fracture toughness, strength and hardness [1,2]. High ionic conductivity at elevated temperature makes it suitable for novel applications like electrolyte in solid oxide fuel cell (SOFC), oxygen probe, etc. [3].

Incorporation of alumina in Y-TZP system affects its mechanical as well as electrical properties. Y-TZP–alumina composite exhibits higher toughness due to the increased transformation volume of Y-TZP by the addition of alumina particles [4,5]. Addition of alumina to zirconia enables the ceramic to exhibit super plasticity during high temperature deformation [6,7]. As far as electrical conductivity of tetragonal zirconia is concerned, there are beneficial effects of addition of alumina [8,9]. However, full exploitation of these advantages can only be realized if the final products having the required specifications comprising desired phase(s), density and microstructure [10–12].

Fabrication of components having such precise mechanical/electrical properties demands tailor-made microstructures and which, in turn demands a proper understanding and control of various processes/processing parameters related to powder synthesis, green stage processing and sintering. Composite powders are difficult to densify as compared to the single phase material due to the retardation of densification by undissolved, non-reactive second phase [5,13]. This problem can be addressed by reducing the starting particle size to nano range. Though nano-scale ceramics are more sinteractive, it is difficult to exploit the full benefit of the initial fine particle size owing to the formation of clusters [14], which consist of primary crystallites, aggregates and agglomerates formed during processing stages. The state of agglomeration influences the

* Corresponding author.
E-mail address: ashok@barc.gov.in (A.K. Sahu).
[1] Present address: School of Chemistry, University of St Andrews, Scotland, UK.

0272-8842/$36.00
doi:10.1016/j.ceramint.2010.11.003

pore size distribution within powder compacts during compaction and thereby, the sintering behaviour of the compacts at a later stage [15]. Aggregates and agglomerates densify more rapidly than the surrounding matrix and, therefore, can give rise to cracks like voids, which cannot be removed by sintering. However, such issues can be addressed by using agglomerate free or soft-agglomerated powder. In the later case, during sintering the matrix shrinks faster compared to agglomerates, thus preventing crack like void formation [16,17].

From the foregoing discussion, it is evident that the powder characteristics (i.e. phase present, particle size and distribution, agglomeration nature, specific surface area, etc.), green density, pore size distribution in powder compacts and sintering conditions (i.e. sintering temperature and soaking time) control the density, microstructure and other related properties of the sintered product. A substantial amount of research on Y-TZP/alumina composite has been carried out by a number of workers, where effects of alumina addition on various properties of the final product have been reported [18–20]. However, many of these reports do not clearly indicate the issue of the effect of various processing parameters on the preparation of material; especially the effect of calcination temperature on the green density and its influence on the sintering behaviour of the composite powder. Hence, the objective of the present investigation is to synthesize nano-crystalline, agglomerate free/soft-agglomerated, sinteractive Y-TZP (2-mol% yttria)–alumina (2 wt%) composite powder and correlate calcinations temperature particle size, green density, sintering temperature with the sintered density. Emphasis is given in the present investigation to study the evolution of green microstructure (i.e. pore size distribution) as a function of calcinations temperature and compaction pressure and its effect on the final densification of the powder compact.

2. Experimental

2 mol% yttria stabilized zirconia with 2 wt% Al_2O_3 (2Y-TZP/Al_2O_3) composite powder was synthesized by reverse strike co-precipitation method, similar to the process used for synthesis of yttria stabilized zirconia by Ghosh et al. [21–23]. In brief, a mixed aqueous solution of zirconium oxy-chloride, yttrium nitrate and aluminium nitrate, containing appropriate amount of cations, was added drop wise into a precipitating bath, consisting of ammoniacal water (pH > 9), polyethylene glycol (PEG) and ammonium sulphate. 10 wt% of each PEG and ammonium sulphate was used to control agglomerate nature of the precipitated precursor. Mechanical stirring of precipitating bath was carried out throughout the process to ensure completion of precipitation with the formation of finely dispersed precipitate. The suspension was decanted and the precipitate was washed thoroughly in aqueous medium to remove undesirable anions, i.e. chloride and sulphate. Subsequently alcohol washing was carried out to remove residual water from the precipitate. The wet cake was dried (in vacuum at 80 °C) and ground.

The thermal decomposition behaviour of the precursor from room temperature to 1400 °C in air was studied by simultaneous thermogravimetric-differential thermal analysis (TG-DTA) technique (Labsys TG, Setaram, France). Based on this result, the precursor powder was calcined at different temperatures in the range of 700–1000 °C.

Calcined powder was ground for 1 h in a planetary ball mill (Fritsch, Germany) using zirconia pot and grinding media. The identification of the phase(s) and the determination of the primary particle size (crystallite size) of the calcined powder were carried out using X-ray diffraction (XRD) (Diano, Series 2000). The conventional Brunnuer Emmet Teller (BET) method was used to measure the specific surface area (Sorptometric-1990, CE Instruments, Italy), using nitrogen gas as adsorbent at liquid nitrogen temperature. This was used to estimate the aggregate size assuming all the particles (aggregates) are spherical in nature. The particle (agglomerate) size distribution of the calcined powder was determined by laser scattering technique (CILAS 1064L, France). The morphology of the calcined powder was examined under a transmission electron microscope (bright field) (TEM) (JEOL 2000 FX, Japan).

The powder calcined at various temperatures was initially compacted uniaxially at low pressure (∼40 MPa) and finally by cold isostatic pressing (CIP) in the range of 50–300 MPa to form green pellets of cylindrical shape. The density of the green pellets was measured by geometric method, taking at least three samples corresponding to each pressure. Porosity and pore-size distribution of a few selected green pellets were measured in a mercury porosimeter (Pascal 440, Thermo Electron, Italy). The shrinkage profile of the iso-pressed (at 300 MPa) green pellets of powders calcined at the four different temperatures, was studied in air at a constant rate of heating (5 °C/min) from room temperature to 1300 °C in a dual push rod type dilatometer (TD 5000S, MAC Science, Japan). For densification study, the powder compacts were sintered isothermally at 1100 °C and 1200 °C for 3 h in air. Density of the sintered samples was measured using Archimedes' principle. The freshly fractured surface of the sample sintered at 1200 °C for 3 h (powder calcined at 800 °C and compacted at 300 MPa) was coated with a thin layer of conducting carbon and observed under a scanning electron microscope (SEM) (Cam Scan MV2300 CT/100, UK).

3. Results and discussion

3.1. TG-DTA study

The simultaneous TG-DTA plot of the precursor material, shown in Fig. 1 exhibits a broad endotherm at ∼130 °C followed by a sharp exothermic peak at 470 °C. The initial endothermic peak could be attributed to the removal of water [24] and organics used during the synthesis of material. Nearly 15% mass loss was observed up to 200 °C whereas the total mass loss recorded up to 1400 °C was ∼23%. This is in good agreement with previously reported values [25–27]. The sharp exothermic peak at 470 °C, could be due to the conversion of amorphous precursor to the crystalline form [27–30].

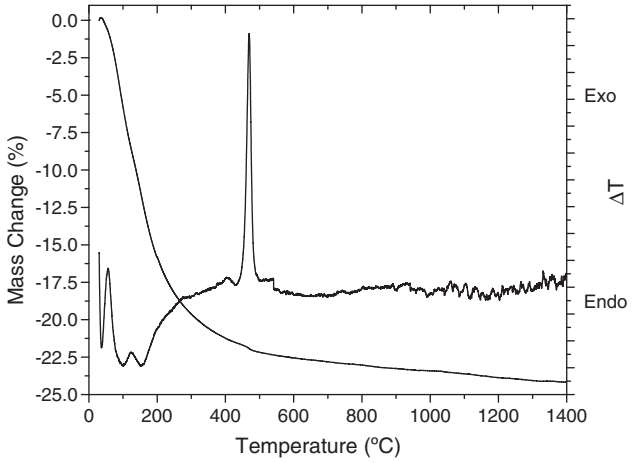

Fig. 1. Thermal decomposition behaviour of the precursor material in air.

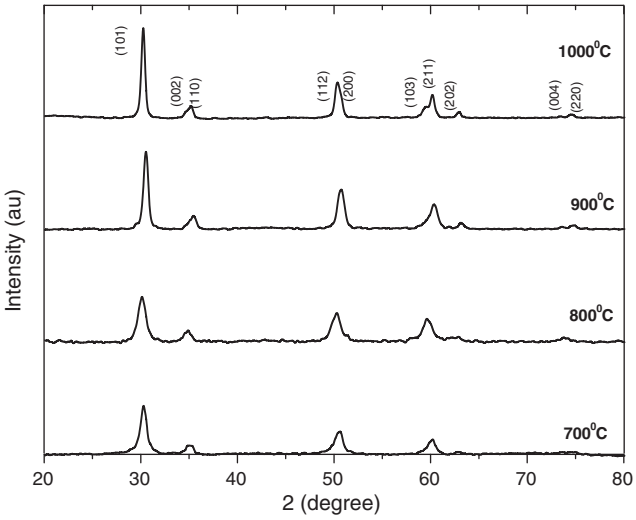

Fig. 2. XRD pattern of 2Y-TZP/2Al_2O_3 powder calcined at different temperatures.

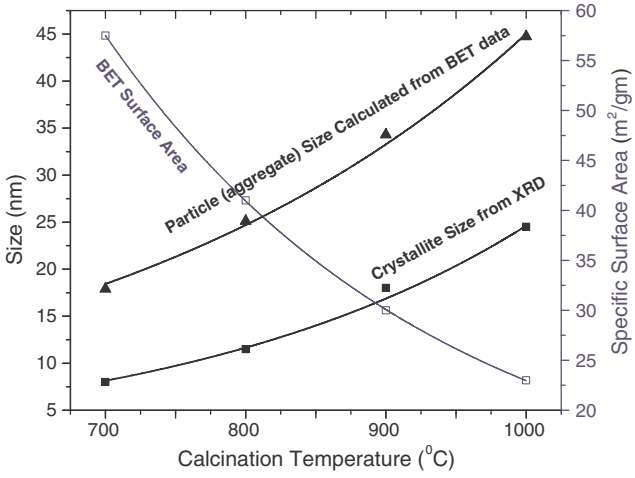

Fig. 3. Variation of specific surface area measured by BET technique, crystallite size measured by X-ray line broadening/particle (aggregate) size calculated from BET data plotted as a function of calcination temperature.

3.2. Characterization of calcined powder

XRD patterns of the powders calcined at four different temperatures in the range of 700–1000 °C, are shown in Fig. 2. These XRD patterns match closely with the one shown in file no. 82-1245 in JCPDS, confirming presence of the tetragonal phase in the powder [31]. The indexing of the XRD peaks has been carried out accordingly. In addition, from the XRD patterns it may be noticed that with increase in calcination temperature the XRD peaks became sharper indicating an increase in the crystallinity and possibly crystallite growth. Since, the quantity of alumina used was 2 wt% (~3 vol%) its presence in the calcined sample was not detected by this technique. Another interesting result was the absence of the monoclinic phase in the calcined samples. Bravo-Leon et al. [1], also observed a similar behaviour in their YSZ-Al_2O_3 system. Although, tetragonal zirconia phase is susceptible to

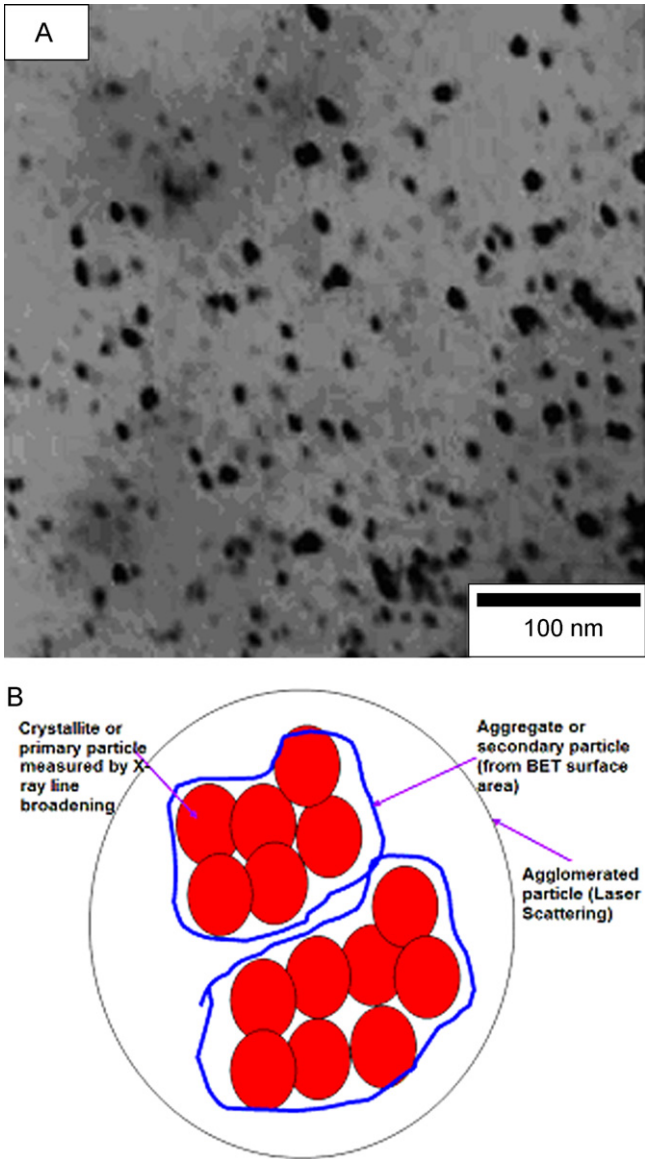

Fig. 4. (A) Representative TEM photomicrograph of powder particle (calcined at 700 °C) and (B) the expected particle nature.

transformation to monoclinic phase below 3 mol% Y_2O_3 doping, but for such spontaneous transformation the size of the primary particle needs to be bigger than a critical size. In the present investigation, the measured crystallite size was below 60 nm in all the cases, which is well below the critical size required for formation of more stable monoclinic phase at room temperature.

The specific surface area of the powder measured by the BET technique was found to decrease with increase in calcination temperature (Fig. 3). An increase in the calcination temperature renders crystallite growth, particle coarsening and/or partial sintering along with neck forming between the crystallite, which leads to the reduction in specific surface area. This observation is also in agreement with the results reported on Y_2O_3–ZrO_2 system [18,32].

The crystallite size measured from broadening of the $(1\ 0\ 1)_t$ peak in XRD patterns, using Scherrer and Warren equation [33], is plotted against calcination temperature in Fig. 3. The figure also shows the variation of aggregate size estimated from the BET data with calcination temperature. An increase in size with the calcination temperature could be observed from the figure. Similar trend was also observed by different researchers for pure tetragonal zirconia, 3 and 10 mol% yttria stabilized zirconia [18,26,34,35].

In the present study the particle (aggregate) size estimated from BET data was found to be nearly double of the crystallite/primary particle size measured by X-ray line broadening technique for a given calcination temperature. The difference in the size estimation could be attributed to the presence of alumina, which retards crystallite growth in the YSZ system and increase the lattice strain [36]. The latter effect is, particularly, responsible for the line broadening in XRD; as a result, the crystallite size estimated from XRD may be smaller than the actual crystallite size. To resolve this issue, the morphology of the calcined and ground powders was observed under a TEM. A representative micrograph is shown in Fig. 4(A). The microstructural features indicate presence of well dispersed particles, especially in the powder sample calcined at lower temperature. The observed particle size was found closer to the values obtained from the BET surface area measurement. Micrographs also indicate the absence of neck formation between particles calcined at lower temperature. The particle size is found to increase with increase in calcination temperature; corroborating aggregate and crystallite size estimated using BET surface area and X-ray line broadening techniques respectively. The real nature of particle is shown in Fig. 4(B). The fine crystallite, during heat treatment not only grows in size, but also may undergo aggregation and form the aggregate or secondary particle. BET surface area, in reality, measures this secondary particle size. The close value of crystallite size and secondary particle size actually indicates the less agglomerated nature of the particle.

The agglomerate size distributions of the calcined and ground powders measured by laser scattering technique (Fig. 5) showed a bimodal distribution for all the samples with an average agglomerate size in the order of ~1.5 μm. This size is much bigger than the crystallite and aggregate size measured by X-ray line broadening (8–23 nm) and BET method (18–45 nm) respectively. This discrepancy could be explained from the fact that laser scattering technique requires aqueous suspension/

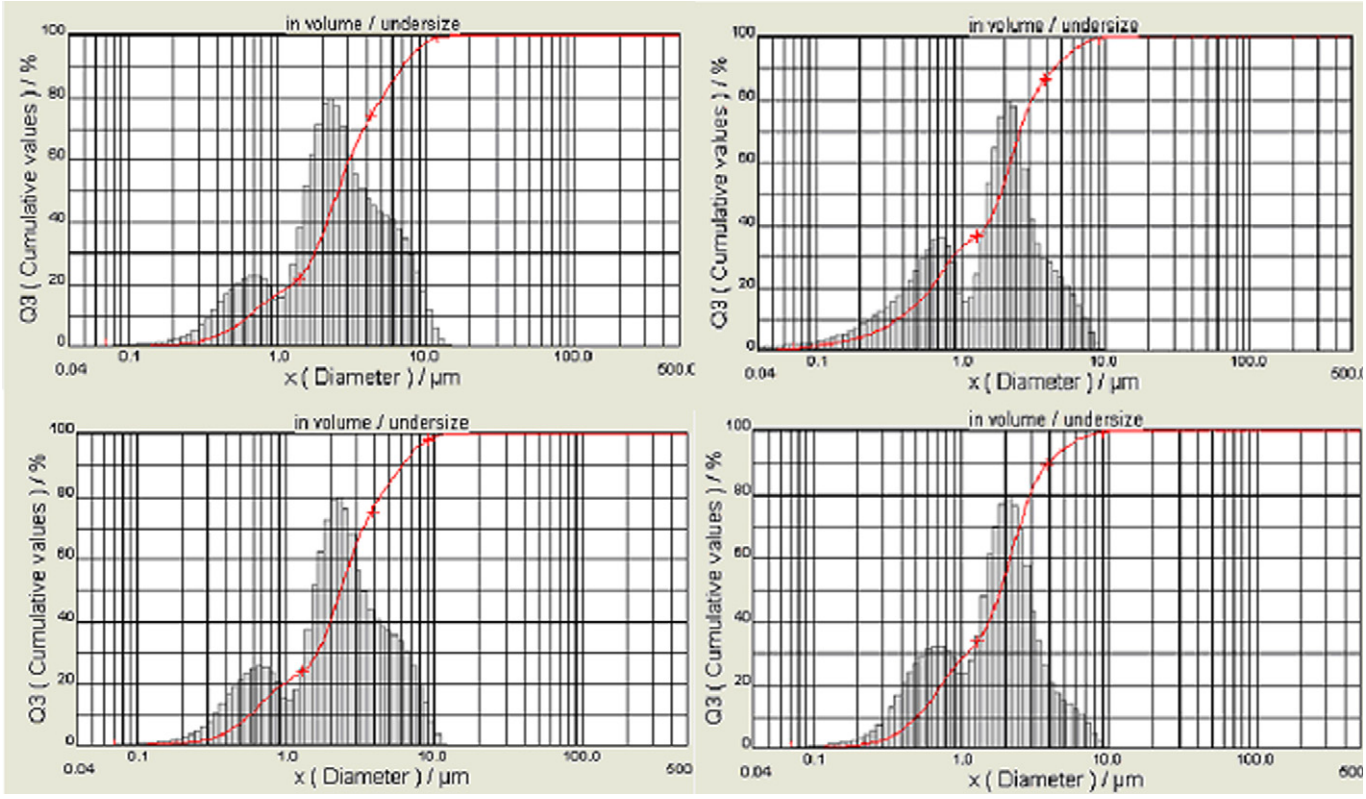

Fig. 5. Agglomerate size distribution (by laser scattering technique) of powders calcined at different temperatures.

dispersion of the powder particles where the formation of agglomerates/flocs is facilitated by the surface tension of water. Thereby the technique inevitably measures the agglomerate size rather than the true particle size [20,37,38].

3.3. Compaction behaviour

The semi-log plot of green density versus compaction pressure is shown in Fig. 6(A). Depending on the calcination temperature and compaction pressure, density was obtained in the range of 37–52%. The rate of increase in density in the low-pressure range (50–100 MPa), as revealed from the plot, is found to be less for all the samples. However, above certain pressure, there is an appreciable increase in density with applied pressure. The situation may be viewed as two straight lines separated by a break point, which is considered as a measure of agglomerate compression strength of the powder [30]. In the present investigation, the strength of the agglomerates was found to be below 100 MPa, indicating the nature of calcined powder to be softly agglomerated.

A linear increase in green density with calcination temperature has been observed for a given compaction pressure (Fig. 6(B)). This may be due to increase in average particle size with calcination temperature, which reduces the number of contact points (per unit volume) amongst themselves, thus the inter-particle friction decreases which results in better compaction. The presence of a clear bimodal particle size distribution (0.1–15 μm) for all the powders calcined at different temperatures further enhances the green compaction by effective pore filling. Similar kind of observation has been reported earlier by Leiser and Whittemore [39] and by Huffine and Bonilla [40].

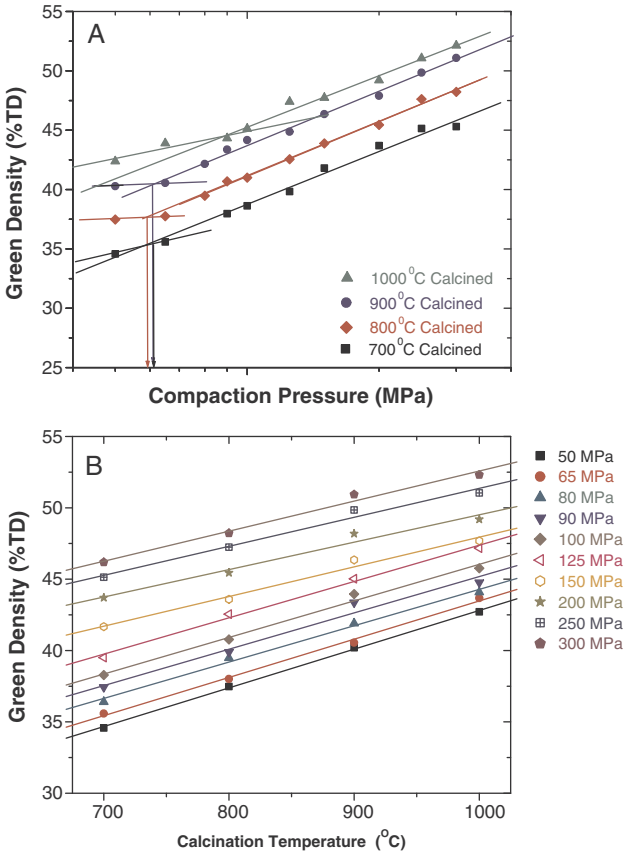

Fig. 6. (A) Green density of powders calcined at various temperatures (700 °C, 800 °C, 900 °C and 1000 °C) is plotted against compaction pressure. The break point (indicated by arrow) in the semi-logarithmic plot indicates the agglomerate strength. (B) Green density plotted as a function of calcination temperature for different compaction pressures.

The pore size distribution of selected green compacts is presented in Fig. 7. A decrease in open porosity with increase in compaction pressure was observed in all the samples. Powders calcined at four different temperatures and compacted at 50 MPa (which was lower than the agglomerate strength of the powder) showed a bimodal pore size distribution. On the other hand, samples compacted above 100 MPa showed a nearly monomodal pore size distribution. As evident from Fig. 7, the cumulative pore volume of the samples decreases with increase in compaction pressure. This indicates a decrease in total porosity in the sample with increase in compaction pressure.

Fig. 7 also shows that the pore size distribution of the sample compacted below the agglomerate strength consisted of one sharp peak followed by a diffused hump, which indicates a wide range of pore size distribution.

The prerequisite of achieving good green density of the powder compact is the fracturing of the agglomerates and their rearrangement. To achieve this, the value of compaction pressure should be more than the strength of the agglomerates. Hence, powders compacted below the value of agglomerate strength showed a wide pore size distribution owing to presence of un-fractured agglomerates. It indicates different pore populations; large pores amongst the agglomerates and smaller one within the agglomerates. Hence, the only means to increase the density at this stage is the rearrangement of agglomerates. This may be a reason for poor densification behaviour observed in the powder compact pressed at the low-pressure range (Fig. 6(A)). The fracturing and rearrangement of the agglomerates at higher pressures are solely responsible for the densification of the powder compact. At this stage, elimination of the inter agglomerate porosity is likely to take place. Fig. 7 shows that the powder compacted at a pressure close to or above the value of its agglomerate strength (∼100 MPa), was devoid of such wide pore size distribution as observed in the powder compacted below the agglomerate strength. With application of higher pressure, the distribution became narrower and almost monomodal in nature. Hence, there is a transition zone from discrete low-pressure agglomerate structure to coherent compact structure at high pressure. The monomodal pore size distribution obtained was the indication of presence of only intra agglomerate porosity, i.e. porosity within the agglomerates. The decrease of pore size with the applied pressure and retaining of monomodal distribution may be due to fracturing of agglomerates and its homogeneous distribution.

The most important requirement for achieving a better sintered-density is to optimize the green density of a highly sinteractive powder. As evident from Fig. 3, size of the primary

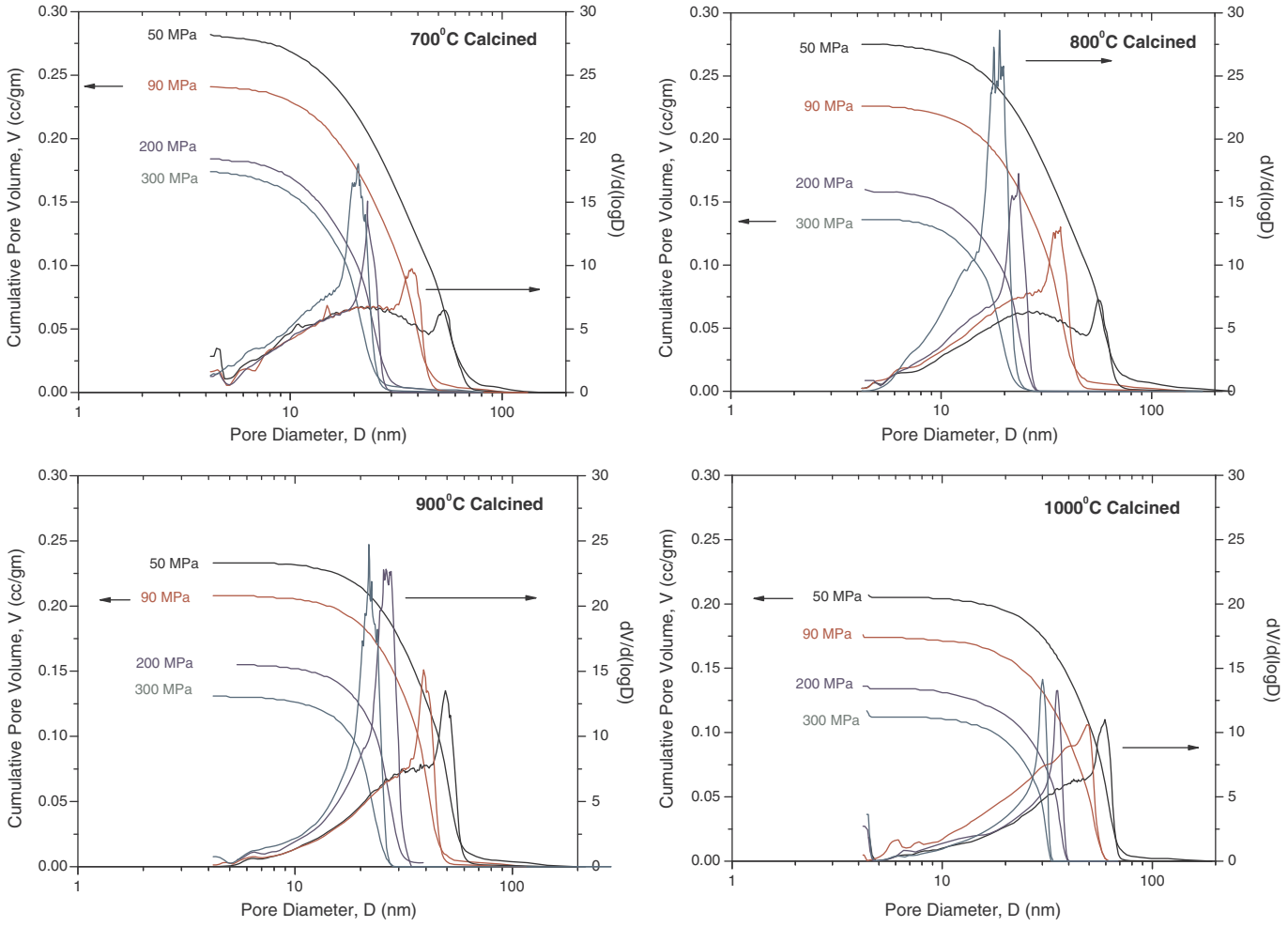

Fig. 7. Cumulative pore-volume (V) and $dV/d(\log D)$ is plotted as a function of pore diameter (D), for powders calcined and compacted at different temperatures and pressures respectively.

as well as aggregated particle was observed to increase with the increase in calcination temperature, thus, the sinteractivity was decreasing. Green density and pore size distribution also play a major role in deciding the densification nature of the power compact. Fig. 7 clearly indicates that samples calcined at 700 °C and 800 °C showed almost similar pore size distribution.

Average pore size (of the green body compacted at 300 MPa) to particle size (aggregate size) (obtained from BET surface area) ratio of the samples is plotted as a function of calcination temperature in Fig. 8. This figure shows that for the sample calcined at 700 °C, the ratio is greater than unity, which indicates, that the pore size is bigger than the particle size; however, for all the other calcined samples, the ratio is less than unity, indicating pores are finer than the particles. According to Kingery and Francois, increase in the pore size to grain size ratio indicates an increase in the pore co-ordination number, i.e. the number of grains present surrounding a pore [41]. Later the works of Lange [42], Kellett and Lange [43] and Shi [44] established a relation between pore stability and pore co-

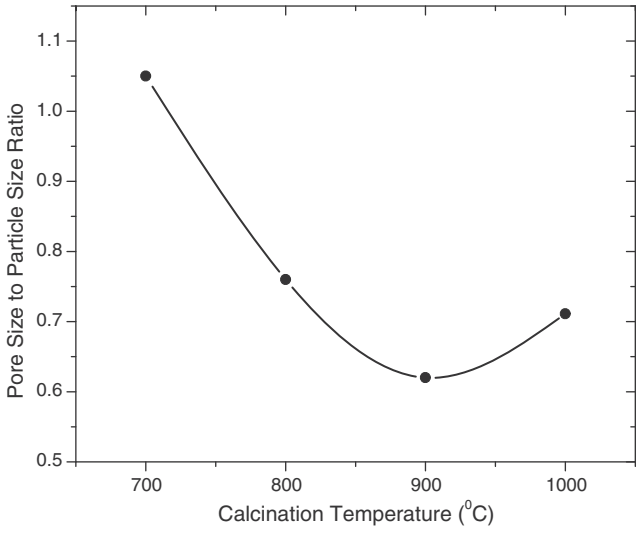

Fig. 8. Ratio of average pore diameter (of the green body compacted at 300 MPa) to the average particle size (calculated from BET data) plotted as a function of calcination temperature.

ordination number. A pore having lower co-ordination number and thus surrounded by concave surfaces (judged from the centre of the pore) is thermodynamically suitable for elimination during sintering, whereas, it is impossible to completely remove convex pores, i.e. pores having higher co-ordination number. Following these approaches, it could be envisaged in the present study that the powder calcined at 700 °C may contain convex pores with higher co-ordination number and thereby may not be thermodynamically suitable for complete elimination; however, powders calcined at higher temperature (i.e. 800–1000 °C) consist of concave pores with lower co-ordination number, which is a more conducive situation for densification.

3.4. Sintering study

The shrinkage profile, i.e. shrinkage (Y) and the rate of shrinkage, i.e. dY/dT are plotted simultaneously as a function of temperature in Fig. 9(A). The shrinkage at 1300 °C was found to decrease from 21% to 17% with increasing calcination temperature. This result compliments the findings of porosimetry, where relatively less amount of pore volume was observed for powder calcined at higher temperature. The differential shrinkage profile of all the samples give a single peak, at 1100 °C corresponding to the maximum rate of sintering. This may be due to homogeneous, monomodal pore size distribution of the green compacts [13,15,45,46].

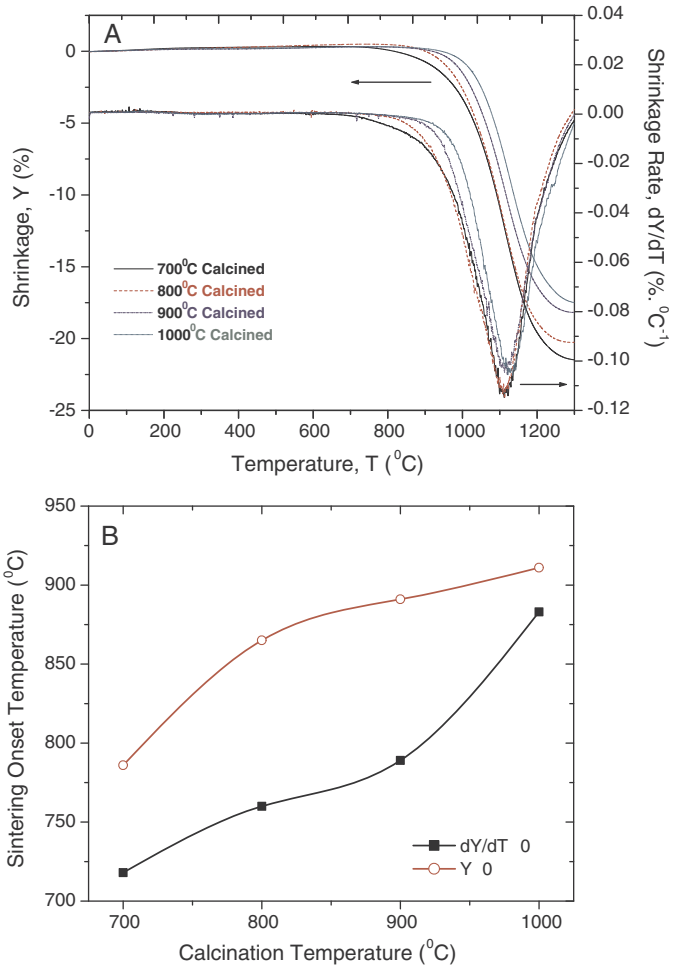

Fig. 9. (A) Shrinkage (Y) and rate of shrinkage (dY/dT) of the green compacts plotted as a function of temperature (measured by constant rate heating experiment) for 2Y-TZP/Al_2O_3 powders calcined in the temperature range of 700–1000 °C. (B) Shrinkage onset temperature (measured from shrinkage profile by tangent intercept method) plotted as a function of calcination temperature.

The onset temperature of sintering is defined as the temperature at which the shrinkage starts. This could be taken as the minimum temperature corresponding to either $Y \leq 0$ (onset of inter-agglomerate/bulk sintering) or $dY/dT \leq 0$ (onset of intra-agglomerate/microscopic sintering). Both of these temperatures were estimated from the shrinkage and differential shrinkage profile by tangent intercept method and plotted as a function of calcination temperature in Fig. 9(B). From this figure it could be seen that the onset temperature of sintering (both bulk and microscopic) increases with calcination temperature. In other words, sinter-activity was found to decrease for the powder calcined at higher temperature. This deterioration of sinter-activity could be due to decrease in specific surface area with increasing calcination temperature.

Density of the samples sintered at 1100°C and 1200 °C for 3 h is plotted as a function of compaction pressure in Fig. 10(A) and (B) respectively. The samples sintered at 1100 °C for 3 h could not achieve good density, whereas, sintering at 1200 °C for the same period of time resulted in nearly full density for the green body compacted at higher pressure. Fig. 10(B) shows that, initially density increases rapidly as a function of compaction pressure. Beyond certain compaction pressure, increase in sintered density with pressure became marginal. The sample calcined at 800 °C had achieved better sintered-density when compacted at higher pressure in comparison to the sample calcined at 900 °C which showed only marginally poorer density compared to 800 °C calcined powder. Surprisingly, 700 °C calcined sample had shown the poorest densification behaviour, although it had the finest particle size. This indicates that particle size alone could not decide the densification behaviour of a powder-compact but the combined effects of particle size and its distribution, green density, pore size and pore size distribution in the powder compact and the average pore size to particle size ratio are all equally critical factors for optimal densification. For a very fine particle size, the number of contact points existing between the particles also increases with decreasing particle size. Such a configuration leads to higher frictional forces between the particles resulting in lower green density. This may have prohibited the 700 °C calcined powder to attain a higher sintered density. A similar observation was made by Laberty-Robert et al. [32], i.e. the sintered density was observed to decrease in case of powders that had the highest specific surface area. In addition, as conjectured before, sample calcined at 700 °C may consist of convex pores with higher co-ordination number, which is not amenable to complete elimination in the course of sintering. At higher calcination temperature, due to grain growth the pore co-ordination number decreases and thereby the pores become unstable [41].

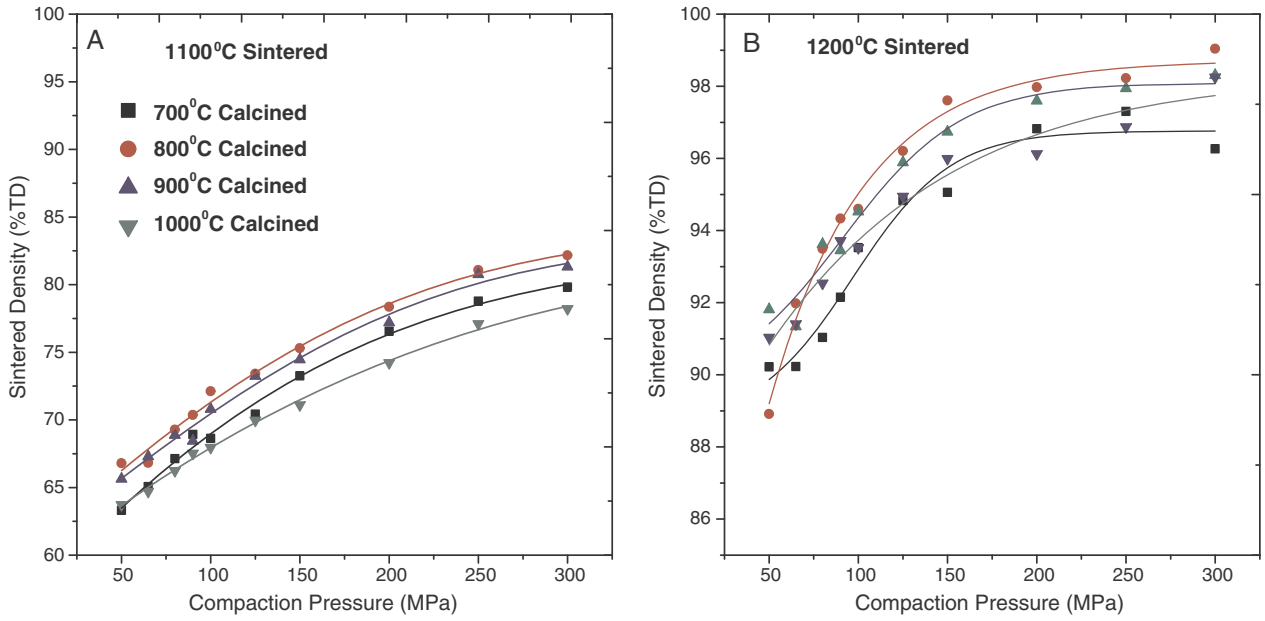

Fig. 10. The density of the samples sintered at (A) 1100 °C and (B) 1200 °C for 3 h, is plotted as a function of compaction pressure.

Only at this situation, the shrinkage of pores takes place leading to densification.

Powder calcined at 800 °C and green compacted at 300 MPa achieved optimal pore size distribution and pore co-ordination number along with suitable specific surface area, which led it to the maximum density after sintering at 1200 °C for 3 h. For powders calcined at higher temperatures (900 °C and 1000 °C), the advantage of lower pore co-ordination number could not be exploited because of less specific surface area with perhaps reduced sinterability of the powders.

A representative photomicrograph of the sample sintered at 1200 °C for 3 h (powder calcined at 800 °C and compacted at 300 MPa) is presented in Fig. 11. It reveals a nearly pore-free dense microstructure with the grain size in the order of sub-micrometer range (~250 nm), which closely matches with the values reported for similar system [1]. This affirms that formation of ultra-fine microstructure is possible through optimization of processing parameters.

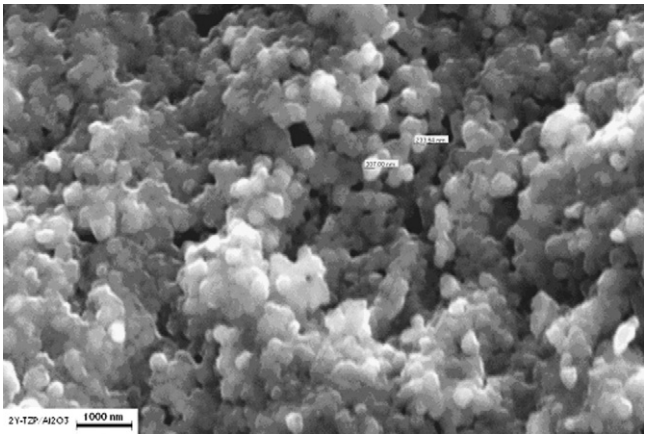

Fig. 11. Scanning electron micrograph of fractured surface of the sample sintered at 1200 °C for 3 h.

4. Conclusions

In the present investigation, it was demonstrated that the synthesis of nano-crystalline 2Y-TZP/Al_2O_3 composite ceramics is possible using a reverse strike co-precipitation method followed by calcination in the temperature range of 700–1000 °C. The size of crystallites (8–23 nm), particles (aggregates, 18–45 nm) and agglomerates (~1.5 μm) measured/estimated using different available techniques and found to increase with the calcination temperature. The green density of the powder compacts was found to increase with calcination temperature and compaction pressure. Both semi-logarithmic plot of green density versus compaction pressure and porosimetry data revealed the soft agglomerated nature of the powder.

The onset temperature of shrinkage of the powder compacts was found to increase with the calcination temperature, i.e. with the increasing particle size. However, in case of isothermal densification, the maximum sintered density (99% of theoretical density) was obtained for an optimal combination of calcination temperature (800 °C), compaction pressure (300 MPa) and sintering temperature (1200 °C) and not for the powder having the finest particles. This observation leads to the fact that particle size (or in other words specific surface area) alone does not determine the densification behaviour of the green body. High specific surface area or fine particle size helps to initiate inter-particular neck formation at relatively lower temperature during heating but for proper pore filling a particular pore geometry (i.e. concave pore surface) is required which is again controlled by the pore to particle size ratio. Hence, particle (aggregate) size (or specific surface area) and pore size to particle size ratio both play critical role in determining the densification behaviour of green compacts. Different processing parameters e.g. calcination temperature, compaction pressure and sintering temperature actually control different microscopic properties like particle size/grain size,

specific surface area and pore size, pore size to particle size ratio, etc. and thereby optimization of these parameters is very essential in order to achieve good sintered product.

References

[1] A. Bravo-Leon, Y. Morikawa, M. Kawahara, M.J. Mayo, Fracture toughness of nanocrystalline tetragonal zirconia with low yttria content, Acta Mater. 50 (2002) 4555–4562.

[2] B.A. Cottom, M.J. Mayo, Fracture toughness of nanocrystalline ZrO_2–3 mol% Y_2O_3 determined by Vickers indentation, Scripta Mater. 34 (5) (1996) 809–814.

[3] A. Hui, J. Roller, S. Yick, X. Zhang, C. Deces-Petit, Y. Xie, R. Maric, D. Ghosh, A brief review of the ionic conductivity enhancement for selected oxide electrolyte, J. Power Source 172 (2007) 493–502.

[4] A.H. Heuer, N. Claussen, W.M. Krive, M. Ruehle, Stability of tetragonal ZrO_2 particles in ceramic matrices, J. Am. Ceram. Soc. 65 (2) (1982) 642.

[5] J.L. Shi, B.S. Li, T.S. Yen, Mechanical properties of Al_2O_3–Y-TZP matrix composite and its toughening mechanism, J. Mater. Sci. 28 (1993) 4019–4022.

[6] K. Tsukuma, T. Takahata, M. Shiomi, Strength and fracture toughness of Y-TZP, Y-TZP/Al_2O_3 and Ce-TZP/Al_2O_3, in: S. Somiya, N. Yamamoto, H. Hanagida (Eds.), Advance in Ceramics, Science and Technology of Zirconia, vol. 24, The Am Ceram Soc, Columbus, OH, 1988, p. 721.

[7] J. Wang, E.M. Taleff, Desiderio Kovar high-temperature deformation of Al_2O_3/Y-TZP particulate composites, Acta Mater. 51 (2003) 3571–3583.

[8] S. Rajendran, J. Drennan, S.P.S. Badwal, Effect of alumina on the grain boundary and volume resistivity of tetragonal zirconia polycrystal, J. Mater. Sci. Lett. 6 (1987) 1431–1434.

[9] Y. Ji, J. Liu, Z. Lu, X. Zhao, T. He, W. Su, Study on the properties of Al_2O_3-doped (ZrO_2)0.92 (Y_2O_3)0.08 electrolyte, Solid State Ionics 126 (1999) 277–283.

[10] T. Sato, S. Shimada, Transformation of yttria-doped tetragonal ZrO_2 polycrystals by annealing in water, J. Am. Ceram. Soc. 68 (1985) 356.

[11] A.J.A. Winnbust, A.J. Burggraaf, The aging behaviour of ultra fine-grained Y-TZP in hot water, in: S. Somiya, N. Yamamoto, H. Hanagida (Eds.), Advance In Ceramic Science and Technology of Zirconia III, vol. 24A, The Am Ceram Soc, Columbus, OH, 1989, pp. 39–47.

[12] J.D. French, M.P. Harmer, H.M. Chan, G.A. Miller, Coarsening-resistant dual-phase interpenetrating microstructures, J. Am. Ceram. Soc. 73 (1990) 2508.

[13] J.L. Shi, J.H. Gao, Z.X. Lin, D.S. Yan, Effect of agglomerate in ZrO_2 powder compacts on microstructural development, J. Mater. Sci. 28 (1993) 328–342.

[14] M.J. Mayo, Processing of nanocrystalline ceramics from ultrafine particles, Int. Mater. Rev. 41 (1996) 85–115.

[15] G.S.A.M. Theuissen, A.J.A. Winnbust, A.J. Burggraaf, Sintering kinetics and microstructure development of nano-scale YTZP ceramics, J. Eur. Ceram. Soc. 11 (1993) 315–324.

[16] B. Kellet, F.F. Lange, Stress induced by differential sintering in powder compacts, J. Am. Ceram. Soc. 67 (1984) 369.

[17] W.F. Dynys, J.W. Halloran, Influence of aggregates on sintering, J. Am. Ceram. Soc. 67 (1984) 596–601.

[18] J.L. Shi, B.S. Li, M.L. Ruan, T.S. Yen, Processing of nano-YTZP/Al_2O_3 composite I: preparation and characterization of nano-YTZP/Al_2O_3 composite powder, J. Eur. Ceram. Soc. 15 (1995) 959–965.

[19] J.L. Shi, J.H. Gao, B.S. Li, T.S. Yen, Processing of nano-YTZP/Al_2O_3 composite II: compaction and sintering behaviour of nano-YTZP/Al_2O_3 composite powder, J. Eur. Ceram. Soc. 15 (1995) 967–973.

[20] O. Vasylkiv, Y. Sakka, V.V. Skorokhod, Low-temperature processing and mechanical properties of zirconia and zirconia–alumina nanoceramics, J. Am. Ceram. Soc. 86 (2) (2003) 299–304.

[21] A. Ghosh, B.T. Rao, T.R. Ramamohan, A.K. Suri, Low-temperature sintering and mechanical property evaluation of nanocrystalline 8 mol% yttria fully stabilized zirconia, J. Am. Ceram. Soc. 90 (7) (2007) 2015–2023.

[22] A. Ghosh, S. Sabharwal, A.K. Suri, B.T. Rao, T.R. Rama Mohan, Synthesis and characterisation of nanocrystalline sinteractive 3Y-TZP powder, Adv. Appl. Ceram. 107 (3) (2008) 170–175.

[23] A. Ghosh, A.K. Suri, B.T. Rao, T.R. Ramamohan, Synthesis of nanocrystalline sinteractive 3Y-TZP powder in presence of ammonium sulphate and poly ethylene glycol, Adv. Appl. Ceram. 108 (2009) 183–188.

[24] B. Aiken, W.P. Hsu, E. Matijevik, Preparation and properties of uniform mixed and coated colloidal particles. Part V. Zirconium compounds, J. Mater. Sci. 25 (1990) 1886–1894.

[25] B. Djuricic, S. Pickering, D. McGarry, P. Glaude, P. Tambuyser, K. Schuster, The properties of zirconia powder produced by homogeneous precipitation, Ceram. Int. 21 (1995) 195.

[26] M.I. Osendi, J.S. Moya, C.J. Serna, J. Soria, Metastability of tetragonal zirconia powder, J. Am. Ceram. Soc. 68 (3) (1985) 135.

[27] M.A. Bleasa, A.J.G. Maroto, S.I. Passaggio, Hydrous zirconium dioxide: interfacial properties, the formation of monodisperse spherical particles, and its crystallization at high temperature, J. Mater. Sci. 20 (1985) 4601–4609.

[28] M. Yoshinaka, K. Hirota, O. Yamaguchi, H. Kume, S. Inamura, H. Miyamoto, N. Shiokawa, R. Shikita, Characterisation and sintering of yttria doped zirconia powders prepared by hydrazine method, Br. Ceram. Trans. 93 (1994) 234–238.

[29] S. Ramanathan, R.V. Muraleedharan, S.K. Roy, P.K.K. Nayar, Dehydration and crystallization kinetics of zirconia–yttria gels, J. Am. Ceram. Soc. 78 (429–432) (1995).

[30] M.A.C.G. Van de Graaf, J.H.H. Ter Maat, A.J. Burggraaf, Microstructure and sintering kinetics of highly reactive ZrO_2–Y_2O_3 ceramics, J. Mater. Sci. 20 (1985) 1407–1418.

[31] Data JCPDS-International Centre for Diffraction, JCPDS-File No. 82-1245, PCPDFWIN v. 2.00, 1998.

[32] C. Laberty-Robert, F. Ansart, C. Deloget, M.A. Gaudon, Rousset dense yttria stabilized zirconia: sintering and microstructure, Ceram. Int. 29 (2003) 151.

[33] B.E. Warren, X-ray diffraction method, J. Appl. Phys. 12 (1941) 375.

[34] S. Ramanathan, N.C. Soni, R. Prasad, Crystallization behaviour of zirconia 10 mol% yttria by hot-stage X-ray diffraction, J. Mater. Sci. Lett. 12 (1993) 122–124.

[35] K. Hishinuma, M. Abe, K. Hasegawa, Z. Nakai, T. Akiba, S. Somiya, Hydrothermal synthesis and properties of yttria fully stabilized zirconia powders, Sci. Technol. Zirconia: Part V (1993) 207.

[36] A.K. Deb, P. Chatterjee, S.P. Sen, S.P. Gupta, Synthesis and microstructural characterization of α-Al_2O_3-t-ZrO_2 composite powders prepared by combustion technique, Mater. Sci. Eng. A 459 (2007) 124–131.

[37] A. Ghosh, Synthesis and Sintering Studies of Yttria Stabilized Zirconia Nano Powders, Indian Institute of Technology, Bombay, Material Processing Division, BARC, Mumbai, vol. PhD. Mumbai, 2006.

[38] D.R. Lazar, C.A.B. Menezes, V. Ussui, A. Helena, A. Bressiani, J.O.A. Paschoal, The influence of sulphur on the processing of zirconia based ceramics, J. Eur. Ceram. Soc. 22 (2002) 2813–2820.

[39] D.B. Leiser, O.J. Whittemore Jr., Compaction behaviour of ceramic particle, Ceram. Bull. 49 (8) (1970).

[40] C.L. Huffine, C.F. Bonilla, Particle-size effects in the compression of powders, AIChE J. 8 (4) (1984) 490–493.

[41] W.D. Kingery, B. Francois, in: N.A. Hooter, G.C. Kuczynski, C.F. Gibbon, S. Gordon, S. Breach (Eds.), Sintering and Related Phenomenon, Gordon & Breach, New York, 1967, p. 471.

[42] F.F. Lange, Sinterabilty of agglomerated powders, J. Am. Ceram. Soc. 67 (1984) 83–89.

[43] B.J. Kellet, F.F. Lange, Thermodynamics of densification. I. Sintering of simple particles, equilibrium configurations, pore stability and shrinkage, J. Am. Ceram. Soc. 72 (5) (1989) 725–734.

[44] J.L. Shi, Solid state sintering of ceramics: pore microstructure models, densification equations and applications, J. Mater. Sci. 34 (1999) 3801–3812.

[45] J. Luo, S. Adak, R. Stevens, Microstructure evolution and grain growth in the sintering of 3Y-TZP ceramics, J. Mater. Sci. 33 (1998) 5301–5309.

[46] E.N.S. Muccillo, R. Muccillo, Physical and electrical properties of yttria stabilized zirconia prepared from nano size powders, Br. Ceram. Trans. 101 (2002) 259–262.